Force Characteristics of an Engaged Involute Gear Tooth

Nesrin Akman, *Member IAENG*

Abstract - An involute gear tooth under repeated pulse loading with varying magnitude as a result of a contact force is analysed. The Euler beam equation allows the deflection at the centre of mass of the gear tooth, modelled as a stubby cantilever, to be calculated. The relationship between the involute angle, axial coordinate and time determines the harmonic function in time to represent the deflection. An equivalent system subjected to a harmonic force representing the component of the contact force causing the deflection is devised. This system comprises a mass matching that of the gear tooth, suspended from a weightless spring and three parallel dampers. The author, after establishing the validity of the model by correctly determining the characteristics of the spring force, hypothesises that one of the dampers acts in a viscous fashion, that the second reacts linearly with the position of the contact force along the gear tooth and that the third, as a harmonic function of time directly proportional to the applied force. Ten gear teeth with involute circle radius varying from 6 mm to 15 mm are modelled and the damping force calculated using the author's hypothesis. The damping force is found to differ to a maximum 0.24 percent of that obtained using the calculated deflection, velocity, acceleration and the contact force.

***Index Terms*— Bending moment, damping force constant, Euler beam equation, involute gear tooth.**

I. INTRODUCTION

The characterisation of the damping forces in a vibrating structure has been actively pursued in structural dynamics [1-4, 9]. The most common approach is to use "viscous damping", where the instantaneous generalized velocities are hypothesized to be the only relevant variables that affect damping forces. Many workers [1, 2, 9, 14] have proposed ways of identifying, from experimental results, damping matrices in linear and multiple-degrees-of-freedom systems. Although these have led to a high degree of confidence in the performance of the matrix, they fail to address the fundamental question of whether the model is indeed correct. Certainly, viscous representation is not the sole model, since all representations with non-negative energy dissipation functional form potential candidates.

In contrast to the forces governing inertia and stiffness, there are questions on the nature of the variables to be included in expressions describing damping. It is generally recognised [1-4] that variables other than instantaneous generalized velocities make a significant contribution, further complicating the model. The existence of high damping forces in structural or mechanical elements leads to additional problems. Here, first order perturbation methods are no longer appropriate.

The author utilises previous research in the structural analyses and studies of the characteristics of gear teeth with respect to spring and damping properties. These are then used to confirm the features of the spring force and establish potential variables that represent the damping force on an involute gear tooth when modelled as a cantilever.

Despite the fact that gear teeth are short and stubby, they still possess elasticity; thus, the deflection of teeth is one of the causes of the transmission error (TE). Case hardened and ground gears are precisely formed, with profile errors of below 4 μm and cumulative pitch errors within 20 μm [5]. Hence, the tooth deflection contributes significantly to the overall relative deviation from smooth running at the mesh point. Loaded non-truly conjugate tooth profiles fail to uniformly transmit angular motion, thus adding to spacing or relative angular placement of driving teeth relative to driven ones. As a consequence, teeth do not engage smoothly and result in high dynamic loads. Then, periodic rather than transient effects determine the maximum load. From the mid-nineties onwards [6, 10- 12], a fruitless search has continued for a modification of profile to eliminate TE. This does not mean that certain modifications which encounter the displacement of gear tooth as a result of bending do not minimize transmission errors. These modifications depend on the magnitude of the contact force and any modification should be minimised. However, any profile adaptation which avoids edge contact at the beginning of mesh is highly desirable.

During the engagement of teeth, energy is dissipated as the lubricant is expelled, adding to the sliding friction. The gear and the pinion, during the engagement, momentarily undergo a pure rolling action as the zone of contact coincides with the pitch point. In all other positions, however, the meshing action is a combination of rolling and sliding. Since rolling resistance is considerably smaller than the latter, its contribution to the total tooth friction is usually neglected. In contrast with the total rolling speed of the gears, the relative sliding velocity [7, 11] varies with the meshing position as well as from one tooth to the other. Vaishya and Singh [13] studied non-linearity and parametric effects in gear dynamics and compared the results of both linear and non-linear time varying systems. They demonstrated that non-linearity in friction exerted its

Manuscript received February 2, 20010.
Nesrin Akman is with the AKM Engineering and Education, 19 Pack Street, Jamboree Heights, QLD 4074, Australia (phone: +61 7 32795692; e-mail: nesrin.akman@akm.com.au).

ISBN: 978-988-18210-8-9 (revised on 5 November 2010) WCE 2010
ISSN: 2078-0958 (Print); ISSN: 2078-0966 (Online)

maximum influence at primary resonance but even then did not significantly contribute to the TE.

Kahraman and Vijayakar [8] highlighted the problems encountered by finite element and semi-analytical deformation treatments when applied to contact zones in planetary gear systems. These are extremely small (typically two orders of magnitude below the working depths of the teeth), and traverse its surface. Their approach uses a finite element model only to compute stresses and relative deformation for points that are away from the contact zones and employs semi-analytical techniques to do the same in the contact zone. The 'near field' semi-analytical, and the 'far field', finite element solutions, are equated at a 'matching surface'. Their model is significantly more difficult to program, but once implemented, provides comparable resolutions to that of a highly refined finite element mesh. Baud and Velex [5] used an extended finite element model. It accounts for flexural torsional axial couplings, mesh stiffness that varies non-linearly with time and departures from the ideal geometry of a tooth. They conclude that the stiffness of the bearing and bending of the shaft must be included in any analysis. Wink and Serpa [15] used three procedures to calculate errors in static transmission of loaded pairs of helical gear pair. They used an incremental procedure with its gradual or iterative application, solving for the distribution of the full load and calculating TE. They reduced the problem via a pseudo interference method and solved it by separate procedures; one by linear programming, the other by a direct matrix solver based on Cholesky factorisation. The later procedure was shown to be highly efficient in solving load distribution problems, encouraging its use in gear strength models that predict contact and bending.

II. INVOLUTE GEAR TOOTH

The tooth profile is created using an involute of circle with radius r. In this application, the value of x is limited to $-r \le x \le r$ requiring φ to be in the range of 2.331 to π radians. The overall length of the tooth is 2r. To avoid the negative values of x, r is added to the value of x, hence moving the origin to the left by r. Similarly, the y value is adjusted by subtracting a constant from it to obtain the thickness of the tooth at the pitch to be equal to $\pi/2P$, where P is the diametral pitch. The parametric equation for such curve is

$$\begin{aligned} x &= r(1+\cos\varphi+\varphi\sin\varphi) \\ y &= r(\sin\varphi-\varphi\cos\varphi)-\left(y_{pitch}-\frac{\pi}{2P}\right) \end{aligned} \qquad (1)$$

Plotting y as a function of x, Fig. 1, shows the tooth profile. When the mating gears engage, the contact force perpendicular to the common tangent to the mating surfaces at the point of contact shown in Fig. 1, is responsible for the bending moment.

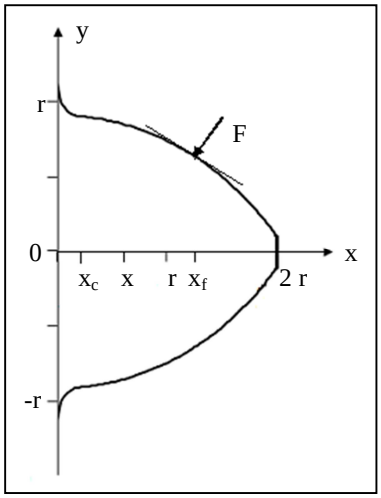

Figure 1: Gear tooth profile

A. Bending Moment

The bending moment $\underline{M}_x$ at x (Fig. 1) due to the y-component ($F_y = F\cos\varphi,$) of the contact force $\underline{F}$ at $x = x_f$ may be written as

$$\underline{M}_x = (x_f - x)\underline{i} \times F_y \underline{j}$$

Substituting for x, x_f and F_y in the equation for $\underline{M}_x$ gives

$$M_x = Fr\cos\varphi_f\left(\cos\varphi_f + \varphi_f \sin\varphi_f - \cos\varphi - \varphi\sin\varphi\right) \qquad (2)$$

During the engagement, the position of the contact force varies from $x_f = 2r$ ($\varphi_f = 2.3311$) at the tip of the tooth to $x_f = x_c$ ($\varphi_f = 3.06$), the beginning of the clearance fillet; the range of horizontal values being the working length of the tooth. The position of the force, x_f, to result a maximum moment at a given value of x varies for $x \le 0.463r$ and remains as the tip for larger values of x. The bending moment at the base, as the force travels along the tooth is shown in Fig. 2; the maximum magnitude occuring at $x = 1.894r$.

If the deflection of the tooth due to the contact force is δ, then

$$\begin{aligned} \frac{EI}{Fr}\frac{d^2\delta}{dx^2} &= M_x \\ &= Fr\cos\varphi_f\left(\cos\varphi_f + \varphi_f \sin\varphi_f - \cos\varphi - \varphi\sin\varphi\right) \end{aligned} \qquad (3)$$

Where E is the Young's modulus and I is the second moment of inertia.

ISBN: 978-988-18210-8-9 (revised on 5 November 2010) WCE 2010
ISSN: 2078-0958 (Print); ISSN: 2078-0966 (Online)

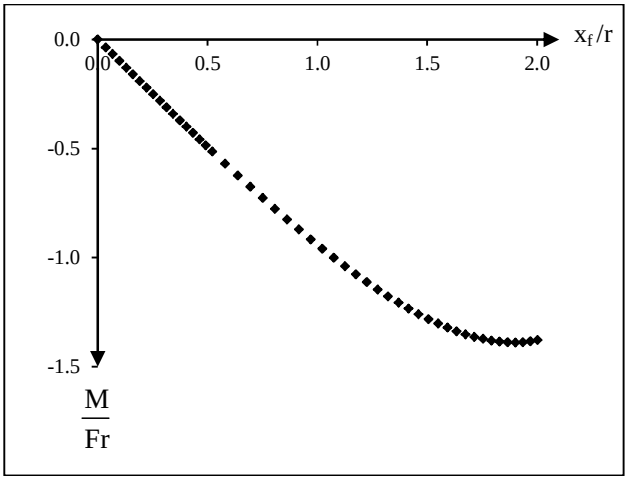

Figure 2: The bending moment at the base of the tooth $(x=0)$ as the force moves along the tooth.

B. Deflection

Integrating the both sides of the above equation and putting $\frac{d\delta}{dx}=0$ at $x=0$ results

$$\frac{EI}{Fr^2}\frac{d\delta}{dx}=\cos\varphi_f\left[\cos\varphi_f\left(\cos\varphi+\varphi\sin\varphi\right)+\varphi_f\sin\varphi_f\left(\cos\varphi+\varphi\sin\varphi\right)-2\varphi\left(\frac{1}{2}\cos\varphi\sin\varphi+\frac{\varphi}{2}\right)-\frac{1}{2}\cos^2\varphi+\frac{\varphi^2}{2}+\frac{1}{2}\varphi^2\cos^2\varphi\right]+\cos^2\varphi_f+\varphi_f\cos\varphi_f\sin\varphi_f+\frac{1}{2}\cos\varphi_f \quad (4)$$

Putting $\frac{d\delta}{dx}=0$ for a given φ gives the position of the force when the maximum deflection occurs. Using the values

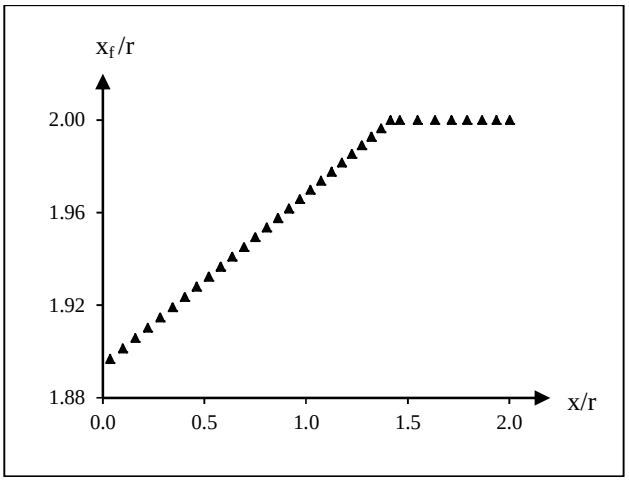

Figure 3: The position of the contact force for maximum deflection along x.

of φ and φ_f, the corresponding values of x and x_f can be calculated. For $x\geq 1.42r$, the maximum deflection occurs when the force is at the tip of the tooth and for $x<1.42$ the position of the force is slightly away from the tip as shown in Fig. 3. Integrating again gives the deflection.

$$\frac{EI}{Fr^3}\delta=\cos^2\varphi_f\left[\varphi\left(\frac{1}{2}\cos\varphi\sin\varphi+\frac{\varphi}{2}\right)+\frac{1}{4}\cos^2\varphi-\frac{\varphi^2}{4}\right]+\cos^2\varphi_f\left[-\frac{1}{2}\varphi^2\cos^2\varphi+\varphi\left(\frac{1}{2}\cos\varphi\sin\varphi+\frac{\varphi}{2}\right)+\frac{1}{4}\cos^2\varphi-\frac{\varphi^2}{4}\right]+\varphi_f\cos\varphi_f\sin\varphi_f\left[\varphi\left(\frac{1}{2}\cos\varphi\sin\varphi+\frac{\varphi}{2}\right)+\frac{1}{4}\cos^2\varphi-\frac{\varphi^2}{4}\right]+\varphi_f\cos\varphi_f\sin\varphi_f\left[\frac{1}{2}\varphi^2\cos^2\varphi+\varphi\left(\frac{1}{2}\cos\varphi\sin\varphi+\frac{\varphi}{2}\right)+\frac{1}{4}\cos^2\varphi-\frac{\varphi^2}{4}\right]-\cos\varphi\left[\frac{1}{3}\varphi^2\cos^3\varphi+\frac{2}{3}\varphi\left(\frac{1}{3}\cos^2\varphi\sin\varphi+\frac{2}{3}\sin\varphi\right)+\frac{2}{27}\cos^3\varphi+\frac{4}{9}\cos\varphi\right]-\frac{1}{2}\cos\varphi_f\left(\varphi^3\sin\varphi+3\varphi^2\cos\varphi-6\cos\varphi-6\varphi\sin\varphi\right)-\frac{1}{2}\cos\varphi\left[\varphi\left(\frac{1}{3}\cos^2\varphi\sin\varphi\frac{2}{3}\sin\varphi\right)+\frac{1}{9}\cos^3\varphi+\frac{2}{3}\cos\varphi\right]+\frac{1}{2}\cos\varphi_f\left[\varphi^3\left(\frac{1}{3}\cos^2\varphi\sin\varphi+\frac{2}{3}\sin\varphi\right)+\frac{1}{3}\varphi^2\cos^3\varphi-\frac{2}{3}\varphi\left(\frac{1}{3}\cos^2\varphi\sin\varphi+\frac{2}{3}\sin\varphi\right)-\frac{2}{27}\cos^3\varphi-\frac{40}{9}\cos\varphi+2\varphi^2\cos\varphi-4\varphi\sin\varphi\right]+\cos^2\varphi_f\left(\cos\varphi+\varphi\sin\varphi\right)+\varphi_f\cos\varphi_f\sin\varphi_f\left(\cos\varphi+\varphi\sin\varphi\right)+\frac{1}{2}\cos\varphi_f\left(\cos\varphi+\varphi\sin\varphi\right)+\frac{1}{3}\cos\varphi_f+\frac{1}{2}\varphi_f\cos\varphi_f\sin\varphi_f+\frac{1}{2}\cos^2\varphi_f \quad (5)$$

The deflection at the tip, as the contact force travels away from it, must be extrapolated since the bending moment at the tip is zero and Eq. 5 is not applicable.

The tooth is subject to the contact force during each cycle for a time period of T/N, where $T=2\pi/\omega$ is the period, N the number of the teeth and ω the angular velocity of the gear. The contact force travels from $x=2r$ to $0.2577r$ – working length of the tooth- during the time period of 0 to $\tau=2\pi/\omega N$. To simplify the dependence between the position of the force and time t, a linear relationship between x and t, as given in Eq. 6 below, is assumed.

$$\frac{x}{r}=\frac{\left(\cos\varphi_c+\varphi_c\sin\varphi_c-1\right)}{2\pi}N\omega t+2 \quad (6)$$

ISBN: 978-988-18210-8-9 (revised on 5 November 2010)
ISSN: 2078-0958 (Print); ISSN: 2078-0966 (Online)

The deflection at $x = x_c$ as a function of time[1], together with its cosine approximation is given in Fig. 4.

The divergence between the two values can be accounted for, by the linear approximation of the horizontal distance covered in a given time. Calculus derived deflections demonstrate its asymptotic approach to zero as the force moves to the base of the tooth (x = 0) which is not the case for the trigonometric approximation.

III. MODELLING

The deflection at the mass centre, as the contact force moves along the tooth, is calculated in terms of the involute angle using Eq. 5. The relationships between the involute angle, axial coordinate, x and time t, then allows the deflection to be expressed as a harmonic function of time. An, equivalent system Fig. 5, subjected to a harmonic force, is devised to model the forces acting on the system. It comprises a mass matching that of the gear tooth, suspended from a weightless spring and three parallel dampers. The author hypothesises that one of the dampers acts in a viscous fashion, that the second reacts linearly with the position of the contact force along the gear tooth and that the third, as a harmonic function of time, directly proportional to the applied force. Ten involute gear teeth with involute circle radius varying from 6 mm to 15 mm are modelled and the damping force calculated using these parallel dampers is found to differ to a maximum 0.24 percent of that obtained using the calculated deflection, velocity, acceleration and the contact force. The spring force constant is found when the system is at rest.

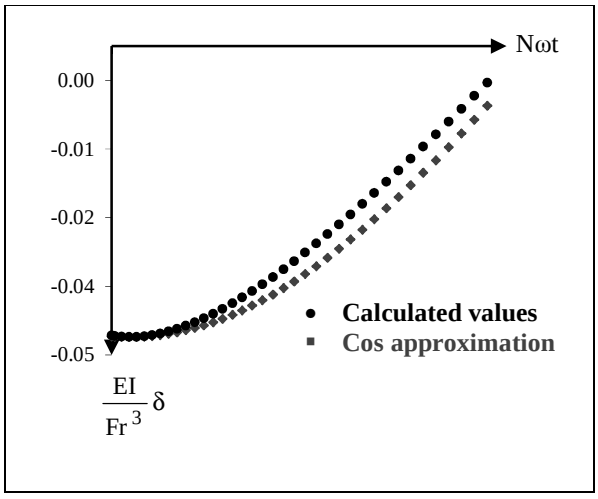

Figure 4: Deflection at $x = x_c$ as a function of time, t.

[1] The deflection at $x = x_c$ rather than at the tip is shown since the deflection at $x = x_c$ is found directly from Eq. 5 as a function of φ and using Eq.s 1 and 6 expressed as a function of time whereas the latter is found through extrapolation.

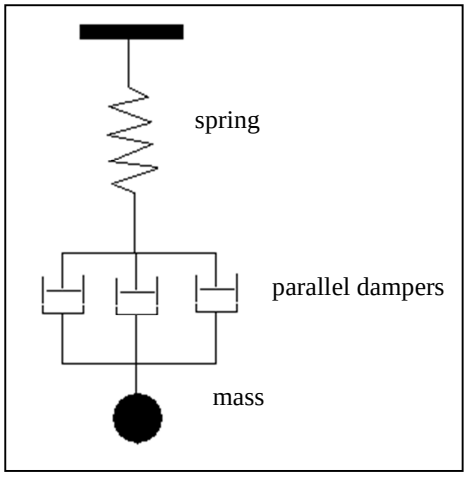

Figure 5: The equivalent system

To simulate the dependence of the deflection on the bending moment, the vertical component of the contact force is multiplied with a scaling function, $f = 1 - \frac{1}{\tau}t$, in the equivalent system. This allows the force to be maximum when the deflection is greatest and be zero at the end of engagement, $t = \tau$.

The equation of motion is

$$m\ddot{\delta} + c\dot{\delta} + k\delta = F_e \qquad (7a)$$

where δ is the displacement.

Now if we define δ as $\delta = F\delta'$, then $\dot{\delta} = F\dot{\delta}'$ and $\ddot{\delta} = F\ddot{\delta}'$.

Substituting in Eq. 7a and dividing each term by the magnitude of the contact force F, gives

$$m\ddot{\delta}' + c\dot{\delta}' + k\delta' = \frac{F_e}{F} \qquad (7b)$$

The ratio of the equivalent and the contact forces, $f_e = F_e/F$, can be written as a periodic function of time.

$$f_e = \cos(bt + d) \qquad (8)$$

where $b = \frac{\varphi_c - \varphi_{2r}}{t_c - t_{2r}}$, $d = \varphi_{2r}$

and φ_c, t_c and φ_{2r}, t_{2r} are the involute angles and time at the clearance and the tip of the tooth respectively.

The departure of the actual and trigonometric approximations of the ratios $f_e = F_e/F$ and F_y/F is accounted for, by the non-linear relationship between x and

ISBN: 978-988-18210-8-9 (revised on 5 November 2010) WCE 2010
ISSN: 2078-0958 (Print); ISSN: 2078-0966 (Online)

time t, although the trigonometci approximation closely approaches the actual one.

A. *Spring Force Constant*

The spring force constant is found when the tooth is at rest. It varies along the tooth as an inverse power function, being infinitely large at the base of the tooth. It increases linearly as the overall height of the tooth increases with increasing base circle radius and as a power function with an index 0.25 with the second moment of inertia (Fig. 6), confirming the validity of the model.

B. *Damping Force Constant*

The variables in the equivalent system are taken as the ratio of the equivalent and the contact forces and ratio of the position of the contact force on the gear tooth to the involute circle radius. The second ratio is needed to take into account that displacement results from the bending moment of the tooth.

The damping force is assumed to be directly proportional to the instantaneous velocity and calculated using the force equilibrium in the equivalent system. Multi variable regression analysis is performed on all ten systems representing the gear teeth with base circle radius ranging from 6 mm to 15 mm (overall length 12 mm to 30 mm) to determine the dependency of the damping force constant on these variables. The constants of the regression equation obtained are given below in Table 1. The adjusted R^2 in each case is 0.99999. The first constant in the analysis is given as the intercept and represents the viscous damping. The second and third constants are associated with the other two dampers in the parallel dashpot.

Next, for each of the ten systems, the damping force constant at each time interval is divided by the fourth root of the second moment of inertia. The multiple regression analysis is repeated for each of the ten equivelant systems and the identical constants obtained are given in Table 2. The adjusted R2 is again 0.99999.

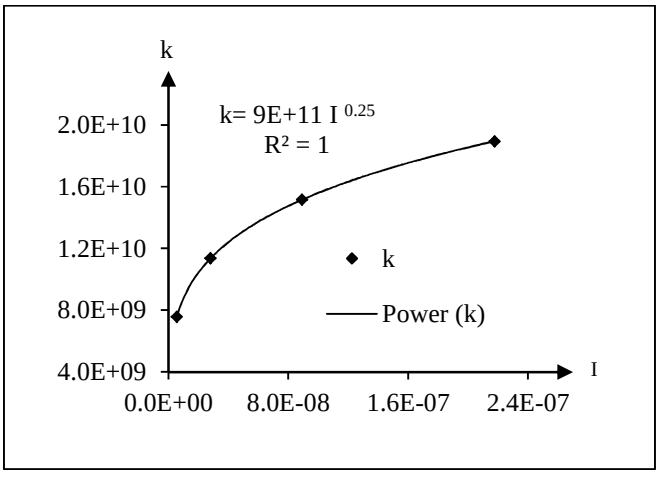

Figure 6: Spring force constant as a function of second moment of inertia.

Table 1: THE MULTI VARIABLE REGRESSION ANALYSIS CONSTANTS FOR THE PARALLEL DAMPERS.

r	viscous	position of f_e	magnitude of f_e
0.006	7978	259137	1216012
0.007	9308	302326	1418680
0.008	10637	345515	1621349
0.009	11967	388705	1824018
0.010	13297	431894	2026686
0.011	14626	475084	2229355
0.012	15956	518273	2432024
0.013	17286	561463	2634692
0.014	18616	604652	2837361
0.015	19945	647841	3040030

Table 2: THE MULTI VARIABLE REGRESSION CONSTANTS FOR THE RATIO OF THE DAMPING FORCE CONSTANT AND THE FOURTH ROOT OF THE SECOND MOMENT OF INERTIA.

R	viscous	position of f_e	magnitude of f_e
6 -15	9.23E+05	3.00E+07	1.41E+08

The multi regression equation for all cases is

$$\frac{c}{I^{0.25}} = 9.23E+05 + 3.00E+07 x_f + 1.41E+08 f_e \qquad (9)$$

Where c = damping force constant
I = second moment of inertia
x_f = the ratio of the position of the force to the base circle radius

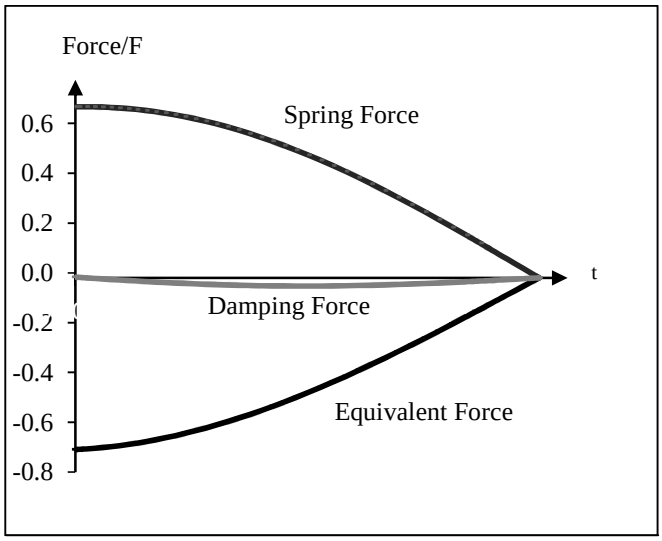

Figure 7: Equivalent, spring and damping forces as a function of time.

ISBN: 978-988-18210-8-9 (revised on 5 November 2010) WCE 2010
ISSN: 2078-0958 (Print); ISSN: 2078-0966 (Online)

The damping force then is written as

$$f_d = (9.23E+05+3.00E+07x_f+1.41E+08f_e)I^{0.25}\,v \quad (10)$$

Where $f_d = F_d/F$ is the ratio of the damping force to the contact force and v is the velocity.

The relevant magnitudes of the spring, damping and equivalent forces are shown in Fig. 7 above. It can be clearly seen that the damping force is much smaller than that of spring force.

IV. Conclusions

There is a particular allure and challenge in determining the variables governing damping forces. Many researchers define kernel functions to fit experimental measurements to their model of damping to obtain damping matrices. These functions ensure non-negative energy dissipation functions. However, they fail to identify the fundamental variables that govern damping.

Here, the Euler beam equation is used to predict the bending moment and deflection of the gear tooth, which is modelled as a two dimensional stubby cantilever. It shows that during the engagement of the tooth, the maximum bending moment fails to occur when the contact force is at the tip without the addendum or tip modification. Additionally, the model demonstrates that the maximum deflection depends on the position of the contact force and corresponds to the contact force being at the tip when measured at two thirds of its height from the base.

An analysis of ten gear teeth with involute of circle radius varying from 6 mm to 15 mm attests that the deflection of the mass centre is close to being a harmonic function of time. The author derives an equivalent system that comprises of a mass matching that of the gear tooth and suspended from a weightless spring and three parallel dampers. This is shown to be subject to a harmonic force derived from the vertical component of the contact force and can adequately be expressed as a function of time.

Multiple variable regression analysis of this system, performed on the ratio of the damping force coefficient and the fourth root of the second moment of inertia, produces a unique set of constants. The first constant termed as the intercept corresponds to the viscous damping. The second and third relate to the position of the contact force on the tooth and the magnitude of the equivalent force correspond to the remaining two dampers. The close fit (by <0.24%) to the resultant damping force from that obtained using the calculated deflection, velocity, acceleration and the equivalent force affirm the legitimacy of the variables chosen.

The spring force constant has been shown to vary along the tooth as an inverse power function, being infinite at its base. It's linear relationship on the overall height of the tooth, together with its dependence the second moment of inertia as a power function with an index 0.25 is demonstrated, confirming the validity of the model. Finally, the damping force has been shown to be much smaller in relation to the spring force and may be neglected in the initial analysis.

The findings are applicable to studies of gear sets such as planetary ones. The mesh stiffness can be written as a non-linear function of time considering the contact ratio and the stiffness of each tooth at the point of engagement together with bearing stiffness. Similarly energy dissipated due to damping may be included in the study using the unique set of constants obtained from the multiple regression analysis.

References

[1] S. Adhikari, J. Woodhouse, Identification of Damping: Part 1, Viscous Damping, Journal of Sound and Vibration, 243(1) (2001) 43-61.
[2] S. Adhikari, J. Woodhouse, Identification of Damping: Part 2, Non-Viscous Damping, Journal of Sound and Vibration, 243(1) (2001) 63-88.
[3] S. Adhikari, Y. Lei, M. I. Friswell, Dynamics of Non-viscously Damped Distributed Parameter Systems, 46th AIAA/ASME/ASCE/AHS/ASC Structures, Structural Dynamics & Materials Conference, Austin, Texas. (2005).
[4] S. Adhikari, On the Quantification of Damping Model Uncertainty, Journal of Sound and Vibration, 306 (2007) 153–171.
[5] S. Baud, P. Velex, Static and Dynamic Tooth Loading in Spur and Helical Geared Systems-Experiments and Model Validation, Journal of Mechanical Design, 124(2) (2002) 334-346.
[6] G. Bonori, B. Barbieri, F. Pellicano , Optimum Profile Modifications of Spur Gears by Means of Genetic Algorithms, Journal of Sound and Vibration, 313 (2008) 603–616.
[7] E. Buckingham, Analytical Mechanics of Gears, General Publishing Co. Ltd., Toronto, 1949, pp. 65-66.
[8] A. Kahraman, S. Vijayakar, Effect of Internal Gear Flexibility on the Quasi-Static Behavior of a Planetary Gear Set, Transactions of the ASME, 123 (2001) 408-415.
[9] N. Larbi, J. Lardies, Experimental Modal Analysis of a Structure Excited by a Random Force, Mechanical Systems and Signal Processing, 14(2) (2000) 181-192.
[10] S. Li, Effects of machining errors, assembly errors and tooth modifications on loading capacity, load- sharing ratio and transmission error of a pair of spur gears, Mechanism and Machine Theory 42 (2007) 698–726.
[11] W. Steeds, Involute Gears, Longmans, Green and Co. London, New York, Toronto, 1948, pp. 121-124.
[12] D. P. Townsend, Dudley's Gear Handbook, Mc Graw Hill, Inc. New York, 1991, pp. 14.11-14.16.
[13] M. Vaishya, R. Singh, Sliding Friction-Induced Non-Linearity and Parametric Effects in Gear Dynamics, Journal of Sound and Vibration, 248(4) (2001) 671-694.
[14] C. Vallee, S. Y. Stepanov , S. Charles, Evaluation Of The Determinant Of Identification Equations For A Linear Model Of A Mechanical Vibratory System, Journal of Applied Mathematics and Mechanics, 69 (2005) 351-357.
[15] C. H. Wink, A. L. Serpa, Performance Assessment of Solution Methods for Load Distribution Problem of Gear Teeth, Mechanism and Machine Theory, 43(1) (2008) 80-94.

ISBN: 978-988-18210-8-9 (revised on 5 November 2010) WCE 2010
ISSN: 2078-0958 (Print); ISSN: 2078-0966 (Online)